Combination strategy targeting VEGF and HGF/c-met in human renal cell carcinoma models.

Combination Strategy Targeting VEGF and HGF/c-met in Human Renal Cell Carcinoma Models

Eric Ciamporcero, Kiersten Marie Miles, Remi Adelaiye, Swathi Ramakrishnan, Li Shen, ShengYu Ku, Stefania Pizzimenti, Barbara Sennino, Giuseppina Barrera, Roberto Pili

Abstract

Alternative pathways to the VEGF, such as hepatocyte growth factor or HGF/c-met, are emerging as key players in tumor angiogenesis and resistance to anti-VEGF therapies. The aim of this study was to assess the effects of a combination strategy targeting the VEGF and c-met pathways in clear cell renal cell carcinoma (ccRCC) models. Male SCID mice (8/group) were implanted with 786-O tumor pieces and treated with either a selective VEGF receptor tyrosine kinase inhibitor, axitinib (36 mg/kg, 2×/day); a c-met inhibitor, crizotinib (25 mg/kg, 1×/day); or combination. We further tested this drug combination in a human ccRCC patient–derived xenograft, RP-R-01, in both VEGF-targeted therapy-sensitive and -resistant models. To evaluate the resistant phenotype, we established an RP-R-01 sunitinib-resistant model by continuous sunitinib treatment (60 mg/kg, 1×/day) of RP-R-01–bearing mice. Treatment with single-agent crizotinib reduced tumor vascularization but failed to inhibit tumor growth in either model, despite also a significant increase of c-met expression and phosphorylation in the sunitinib-resistant tumors. In contrast, axitinib treatment was effective in inhibiting angiogenesis and tumor growth in both models, with its antitumor effect significantly increased by the combined treatment with crizotinib, independently from c-met expression. Combination treatment also induced prolonged survival and significant tumor growth inhibition in the 786-O human RCC model. Overall, our results support the rationale for the clinical testing of combined VEGF and HGF/c-met pathway blockade in the treatment of ccRCC, both in first- and second-line setting. *Mol Cancer Ther; 14(1); 101–10. ©2014 AACR*.

Introduction

Renal cell carcinoma (RCC) strikes approximately >64,000 people and causes >13,000 deaths in a year in the United States (**1**). Approximately 80% of RCC cases are diagnosed as clear cell RCC (ccRCC) and the majority of them are sporadic tumors with acquired defects in both alleles of VHL (von Hippel-Landau) tumor-suppressor gene, resulting in VHL protein dysregulation (**2**). This defective protein is unable to bind under hypoxic conditions, and trigger proteasome-mediated degradation of hypoxia-inducible transcription factor (HIF). The subsequent transcriptional hyperactivation of HIF-targeted genes, such as VEGF, platelet-derived growth factor (PDGF), TGFα, hepatocyte growth factor (HGF), and mesenchymal–epithelial transition factor (MET), drives tumor progression and hypervascularization (**3–5**).

Anti-VEGF drugs have been shown to have a great therapeutic benefit in patients with ccRCC. The VEGF pathway does play a pivotal role in tumor angiogenesis and its overactivation is often associated with tumor growth and metastases (**6**). Among the VEGF-targeted therapies FDA approved as frontline treatment for advanced RCC, tyrosine kinase inhibitors (TKI) represent the most common choice (**7**). Because of their mechanism of action at the ATP-binding site, TKIs are selective rather than specific for a single kinase. Sunitinib, in particular, has been shown to inhibit PDGF receptor (PDGFR), v-kit Hardy–

Zuckerman 4 feline sarcoma viral oncogene homolog (c-kit) and VEGF receptors 1 and 2 (**8**). Albeit these multi-TKIs can be highly effective by targeting more than one oncogenic pathway, a selective and potent VEGFR TKI may improve effectiveness and decrease the adverse events often observed in patients treated with multitarget small molecules. Axitinib (former AG-013736) is a potent small-molecule TKI, highly selective for VEGF receptor 1, 2, and 3 has been approved as a second-line treatment for RCC and is currently being tested in phase II/III clinical trials for the treatment of solid tumors (**9, 10**). Axitinib advantages include a well-tolerated clinical safety profile and a relative short half-life (2–5 hours) that allows dose adjustment/titration (**11**).

VEGF-targeted therapies elicit survival benefit in RCC, but fail to produce enduring clinical responses in most patients. Indeed, inevitably, disease progresses following a transient 9- to 11-month period of clinical benefit. Among the different mechanisms of evasive resistance to antiangiogenic therapies, the upregulation of alternative proangiogenic signals, and an increase of the invasive and metastatic behavior of tumor cells have been reported to play an important role (**12, 13**).

The HGF/MET factor (c-met) pathway has been shown to be relevant in acquired drug resistance as well as in tumor vascularization, epithelial-to-mesenchymal transition, and metastases (**14**). C-met is one of the most deregulated receptor tyrosine kinase (RTK) in advanced cancers and MET-activating mutations are the genetic cause of hereditary papillary type I RCC and other cancers (**15**). Intriguingly, c-met is transcriptionally activated by hypoxia and acts as mediator of antiangiogenic therapy resistance in models of glioblastoma multiforme (**16, 17**) and other solid tumors (**18**). Crizotinib (also known as PF-2341066) is an orally available, potent, and selective dual inhibitor of anaplastic lymphoma kinase (ALK) and c-met kinase that has been approved for the treatment of ALK-positive non–small cell lung cancers (**19, 20**).

The aim of this study was to test the antitumor efficacy of axitinib and crizotinib combination in ccRCC models. The data suggest that combination with crizotinib increases axitinib induced antiangiogenic and antitumor activity in both TKIs sensitive and TKIs resistant models.

Materials and Methods

Compounds

Axitinib (AG013736 or Inlyta), crizotinib (PF-02341066 or Xalkori), and sunitinib (Sutent) were provided by Pfizer. For *in vivo* formulations, axitinib was prepared in 0.5% carboxymethylcellulose solution and crizotinib was dissolved in water by pH adjustment to a value between 3.5 and 4. Drugs were administered by oral gavage (*per os* or PO). The experimental groups were the following: vehicle (0.5% carboxymethylcellulose, 2×/day, 5×/week, PO), axitinib (36 mg/kg, 2×/day, 5×/week, PO), crizotinib (25 mg/kg, 1×/day, 5×/week, PO), axitinib plus crizotinib combination (same schedule and concentration as in single-agent groups). Treatments were administered as follows: 4 weeks (786-O 1-month endpoint), 6 weeks (RP-R-01 sunitinib resistant), 10 weeks (RP-R-01 sunitinib sensitive), or up to 15 weeks (786-O survival). Mouse body weight and tumor caliper measurements were taken weekly. No overt signs of toxicity were observed in any treatment group (i.e., significant weight loss or diarrhea).

Xenograft models and treatment protocol

Immunodeficient SCID male mice purchased from Roswell Park Cancer Institute (RPCI) were used for these studies and all procedures were approved by the Institute Animal Care and Use Committee. Mice were kept in a temperature controlled room on a 12 of 12 hours light/dark schedule with food and water *ad libitum*. Collection of tumor samples was obtained via regulatory approval at the institution.

786-O cells were purchased from the ATCC. Mice (8/group) were implanted under the right kidney capsule with approximately 1-mm^3 size tumor pieces derived from previously orthotopically implanted, untreated 786-O tumors. Treatments began approximately 5 weeks later, when tumors were detectable by palpation, and followed the schedule described above. 786-O survival study: 32 mice (8/group) were implanted and treated as described above. Animals were monitored twice daily for health issues, moribund mice were euthanized by CO^2 asphyxiation and deaths were recorded for each mouse. Each animal found dead or euthanized was necropsied. Criteria for euthanasia were based on an independent assessment by a veterinarian according to AAALAC guidelines and only cases in which the conditions of the animal were considered incompatible with life were reported as deaths. As a control of good surgical procedure, we performed necropsies on mice survived until the end of treatment and tumors were found to be present under the right kidney capsule in all of the cases.

RP-R-01 is a patient-derived xenograft model developed from a skin metastasis of a patient with sporadic ccRCC $VHL^{-/-}$ developed while on sunitinib treatment, as previously described (**21**). This model was propagated *in vivo* only to maintain the heterogeneity of the primary tumor. The short-term study: mice (3/group) were implanted subcutaneously in the flank area with approximately 4-mm^2 size RP-R-01 tumor pieces. Treatment started when average tumor dimension reached approximately 35 mm^2: Mice were randomized in the above-mentioned experimental groups and treated for either 2 or 7 days. Because previous studies performed in our laboratory showed good antitumor efficacy of sunitinib in this model, we implanted mice (8/group) subcutaneously with RP-R-01 tumor pieces, as described above, as models of sunitinib-sensitive human ccRCC. Treatment started when average tumor dimension reached approximately 50 mm^2. To establish a sunitinib-resistant model, we implanted 35 mice subcutaneously in the flank area with approximately 4- to 5-mm^2 size RP-R-01 tumor pieces and, approximately 6 weeks later, when tumors reached an average size of approximately 25 mm^2, mice were treated with sunitinib (60 mg/kg, 5×/week, PO). We defined resistant tumors when they reached doubled size upon treatment (~50 mm^2). Thereafter, mice were divided into homogenous groups (7 mice/group) as determined by caliper measurements and randomized to the above-mentioned experimental groups. Mice in all experiments have been sacrificed between 12 and 18 hours after last treatment.

Immunohistochemistry

Tissues were fixed for 24 hours in 10% neutral-buffered formalin (c-met E-cadherin and Ki67) or zinc fixative (CD31), paraffin embedded and cut at 4 µm, placed on charged slides, and dried at 60°C for 1 hour. Slides were cooled to room temperature, deparaffinized in xylene, and rehydrated using graded alcohols. Antigen unmasking was heat mediated, in citrate buffer (pH 6.0) and followed by a 20 minutes cool down. Endogenous peroxidases were quenched with 3% H_2O_2 for 10 minutes and washed with PBS-Tween20 0.1%. Slides were then blocked for 1 hour with PBS 1% BSA and incubated overnight in primary antibodies: Mouse CD31 (1:100, 550274; BD Pharmingen), c-met (1:300, 8198; Cell Signaling Technology), E-cadherin (1:400, 3195; Cell Signaling Technology), or Ki67 (1:500; Thermo Scientific RM-9106). Sections were then incubated in horseradish-conjugated anti-rabbit (E-cadherin, c-met, and Ki67) or anti-rat (CD31) antibody according to the manufacturer's protocol (Vector Laboratories) followed by enzymatic development in diaminobenzidine (DAB). Slides were finally counterstained with hematoxylin, dehydrated, and mounted with cytoseal 60 (Thermo Scientific). Quantification of the staining was performed by using ImageJ software in a blinded fashion by analyzing four randomly selected fields per tissue of six to eight samples per treatment. CD31, E-cadherin, and c-met results are expressed as the average percentage of positive area per treatment ± SE; Ki67 as the percentage of positive nuclei per treatment ± SE calculated by Immunoratio plugin for ImageJ (**22**).

Immunofluorescence

Tissues were snap-frozen and stored at −80°C, 10-μm thick sections were cut with a cryostat and placed in positively charged slides. Sections were then fixed for 10 minutes at −20°C in PBS-4% paraformaldehyde solution and washed–permeabilized in PBS 0.3% Triton X-100. Phosphorylated c-met staining was adapted from the protocol described by Sennino and colleagues (**23**): Slides were blocked for 1 hour with immunomix (PBS 0.3% Triton X-100, 5% normal horse serum, 0.2% BSA) and incubated in primary c-met phosphorylation-specific antibody overnight at room temperature (pYpYpY$^{1230/1234/}$1235, 1:250, 44888G; Invitrogen). Following primary incubation, sections were incubated with FITC-conjugated anti-rabbit antibody for 1 hour at room temperature in a humidified dark chamber. Cy3 goat anti-rat (Invitrogen) was used to detect the anti-CD31 antibody in the dual color fluorescence experiments. Immunocomplexes were then briefly fixed for 5 minutes in 1% paraformaldehyde, nuclei stained with DAPI, and slides mounted with vectashield mounting medium (Vector Laboratories). The number of phosphorylated c-met–positive cells was counted in a blinded fashion by analyzing at least six randomly selected 40× fields per tissue of six samples per treatment.

Intratumoral hypoxia detection

At the end of treatment, mice in the RP-R-01 short-term experiment were injected i.p. with 60 mg/kg pimonidazole hydrochloride (Hypoxiprobe plus kit), and 1 hour later, mice were euthanized. To stain hypoxic areas, we followed the protocol described for immunofluorescence, using 4.3.11.3 mouse-FITC MAb1 according to the manufacturer. The percentage of hypoxic area was counted in a blinded fashion by analyzing at least six randomly selected 10× fields per tissue of three samples per treatment.

Statistical analysis

Differences among experimental groups were tested by either the Student *t* test or for variances by ANOVA. A *P* value of <0.05 was considered statistically significant. The difference in tumor weight between treatment groups was statistically evaluated by nonparametric the Mann–Whitney*U* test.

Results

Antitumor effect of axitinib and crizotinib in the 786-O orthotopic model

To examine the therapeutic effect of axitinib and crizotinib in the high c-met–expressing 786-O model (Supplementary Fig. S1A), male SCID mice were orthotopically implanted under the kidney capsule with tumor tissues. When tumors became detectable by palpation, mice were randomized to treatment with either vehicle, axitinib, crizotinib, or combination. After 4 weeks, mice were sacrificed and tumors were excised and weighed. Although tumor weights in both single-agent groups were smaller than in vehicle-treated mice (17% overall reduction in axitinib and 10% in crizotinib), no statistical differences were observed. However, the average tumor weight in the combination group was significantly smaller as compared with single-agent groups ($P = 0.0292$ vs. axitinib and $P = 0.0321$ vs. crizotinib) and the vehicle group ($P = 0.0004$), showing a 76% overall reduction as compared with the vehicle group (**Fig. 1A**). Ki67 staining did not show significant differences in the proliferative index among groups in this highly proliferative model (data not shown). Microvessel density analysis by CD31 staining revealed, as expected, a reduction in tumor vascularization following treatment with either axitinib ($P < 0.0001$) or crizotinib (**Fig. 1C and D**). Noteworthy, tumor vascularization was further reduced following combined treatment ($P = 0.0040$ vs. axitinib and $P < 0.0001$ vs. both vehicle and crizotinib single agent).

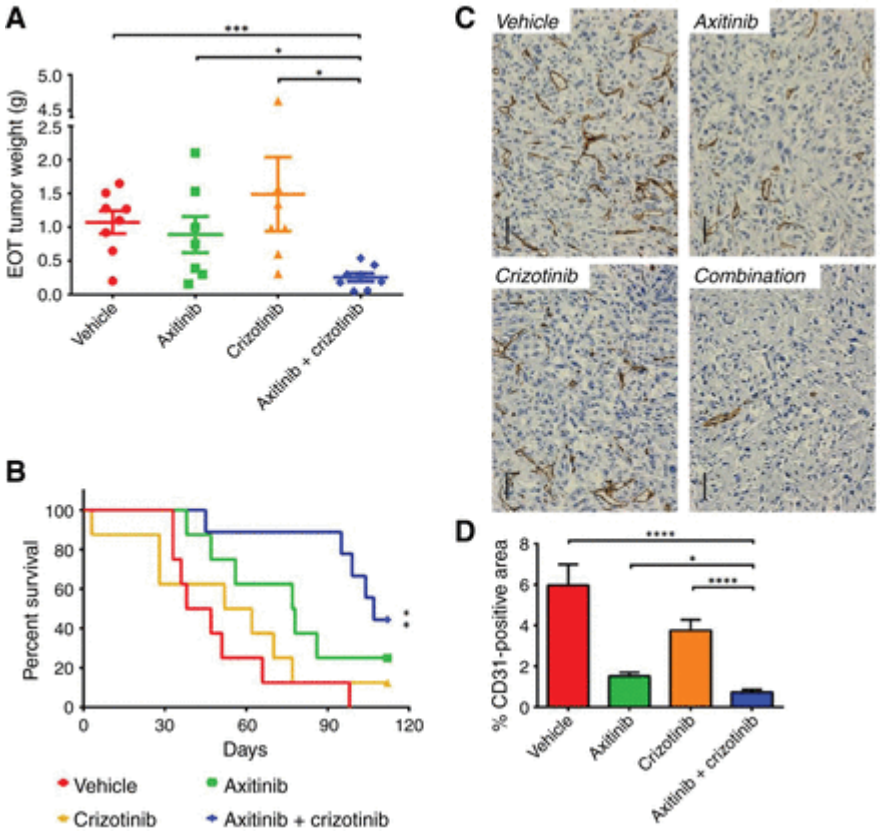

Figure 1.

Antitumor effect of axitinib and crizotinib in the 786-O orthotopic model. Mice orthotopically implanted with 786-O tumor pieces (8 mice/group) were treated for 4 weeks with vehicle, axitinib (36 mg/kg, 2×/day, 5×/week), crizotinib (25 mg/kg, 1×/day, 5×/week), or combination. A, endpoint tumor weight: each point represents one tumor; bars, average of each treatment group ± SE; *, $P < 0.05$ and ***, $P < 0.001$, as compared with the combination group, using two-tailed *t* test analysis. EOT, end of treatment. B, Kaplan–Meier survival curve of mice orthotopically implanted with 786-O tumor pieces and treated as described above. The vertical ticks, censoring times; **, $P < 0.01$ calculated by the log-rank test. C, tumors from mice treated as in A were harvested, processed, and tissue sections were stained for CD31 for visualization of endothelial cells. D, blinded quantitative analysis of CD31, expressed as the mean percentage of positively stained area ± SE; *, $P < 0.05$ and ****, $P < 0.0001$, as compared with the combination group, using two-tailed *t* test analysis.

Then, in view of the combinatorial antitumor effect of axitinib and crizotinib, we conducted a survival experiment involving 786-O tumors orthotopically implanted in mice treated as described above. Kaplan–Meier survival curves show an increase in median survival in both single-agent–treated mice as compared with vehicle (42.5 days in vehicle, 77.5 in axitinib, 57 in crizotinib; **Fig. 1B**). At end of the approximately 4-month experiment, combination treatment resulted in a statistically significant improvement and extension of survival (median survival, 107 days; log-rank test, $P = 0.0045$).

Axitinib and crizotinib short-term treatment in the sunitinib-sensitive RP-R-01 PDX model

To evaluate the efficacy of axitinib and crizotinib in another sunitinib-sensitive but low c-met expression model (Supplementary Fig. S1A), SCID mice were implanted with the ccRCC PDX RP-R-01. Tumors were measured weekly with a caliper and, when the average tumor dimension reached approximately 35 mm^2,

mice were randomized into eight groups and treated with either vehicle, single agents, or combination for either 2 or 7 days. At either time points, average tumor dimension was not significantly different among groups (Supplementary Fig. S1B and S1C). Despite homogenous tumor dimension among groups, tumor vascularization was already reduced after 2 days of axitinib treatment (**Fig. 2A**). Crizotinib single-agent treatment did not affect blood vessel density, but combination treatment displayed a stronger reduction of CD31-positive area, significantly lower than each other group after 7 days of treatment (P = 0.0159 vs. vehicle, P = 0.0404 vs. axitinib, and P = 0.0357 vs. crizotinib, **Fig. 2C**). In agreement with this significant reduction in tumor vascularization, pimonidazole staining (**Fig. 2B**) displayed a statistically significant increase in intratumor hypoxia in the combination group already at day 2 (P = 0.0400 vs. vehicle, **Fig. 2D**). Furthermore, at day 7, also axitinib (P = 0.0394) and crizotinib (P = 0.0642) single agents showed an increased intratumor hypoxia compared with the vehicle group but, again, also at this time point the extent of combined treatment-induced hypoxia was greater (P = 0.0009). As expected, the immunodetection of the phosphorylated c-met (Tyr$^{1230/1234/1235}$) displayed a substantial reduction in the number of positive cells in the tumors treated with crizotinib (Supplementary Fig. S1D and S1E). CD31–pimonidazole dual-color immunofluorescence highlighted an obvious induction of hypoxia in all three treated groups, originating surprisingly from the blood vessels (with an overall more robust effect in the combination group, Supplementary Fig. S2A). As shown in Supplementary Fig. S2B, endothelial cells of the tumor blood vessels display phosphorylated c-met staining at least equal to RP-R-01 cancer cells, making also them a putative crizotinib target.

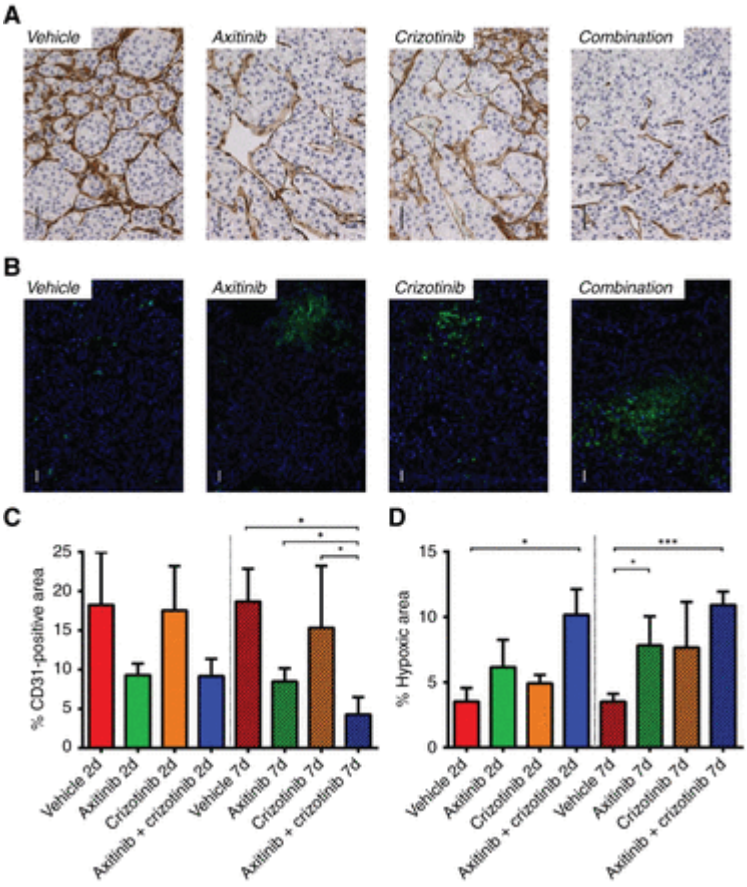

Figure 2.

Axitinib and crizotinib short-term treatment in the sunitinib-sensitive RP-R-01 PDX model. Subcutaneous RP-R-01–bearing mice (3/group) were treated with vehicle, axitinib (36 mg/kg, 2×/day), crizotinib (25

mg/kg, 1×/day), or combination for either 2 (labeled as 2d) or 7 days (7d). Tumors were then harvested, processed, and tissue sections were stained by IHC for CD31 (A), to display endothelial cells and pimonidazole by immunofluorescence (green; B), to assess intratumor hypoxia (DAPI counterstain marks nuclei in blue); scale bar, 50 μm. Blinded quantitative analysis of tumor vascularization (C) and intratumor hypoxia (D), expressed as the mean percentage of positively stained area ± SE; *, $P < 0.05$ and ***, $P < 0.001$, using two-tailed *t* test analysis (the vertical spotted lines highlight the difference in time among groups).

Antitumor effect of axitinib and crizotinib in the sunitinib-sensitive RP-R-01 PDX model

To assess the antitumor efficacy of axitinib and crizotinib in RP-R-01, we performed also a long-term treatment experiment. When the average tumor dimension reached approximately 50 mm^2, mice were randomized into four groups and treated with either vehicle, single agents, or combination. Tumor growth in mice treated with either crizotinib or vehicle was similar and mice were sacrificed after 40 days of treatment (**Fig. 3A**). Treatment with axitinib single agent significantly decreased the growth of tumors, but combination with crizotinib further enhanced axitinib antitumor efficacy. After 70 days of treatment, tumors in the combination group were significantly smaller than in the axitinib group ($P = 0.0474$ for tumor dimension and $P = 0.0490$ for tumor weight; **Fig. 3B**). Ki67 staining confirmed the inhibition of tumor proliferation in both axitinib and crizotinib groups ($P < 0.0001$ vs. vehicle; **Fig. 3C and E**). **Figure 3D** shows representative CD31 staining of tumor tissues. We observed a significant reduction in tumor vascularization in both axitinib and combination groups ($P < 0.0001$ vs. vehicle), although comparison between these two groups was not significant. Blood vessel reduction in crizotinib-treated tumors as compared with the vehicle group was modest and not statistically significant (**Fig. 3F**). IHC for c-met did not show any significant difference in expression among the experimental groups (Supplementary Fig. S3A and S3C). Furthermore, neither c-met phosphorylation ($Tyr^{1230/1234/1235}$) increase in the axitinib-treated group and decrease in the crizotinib-treated group were statistically significant (Supplementary Fig. S3B and S3D).

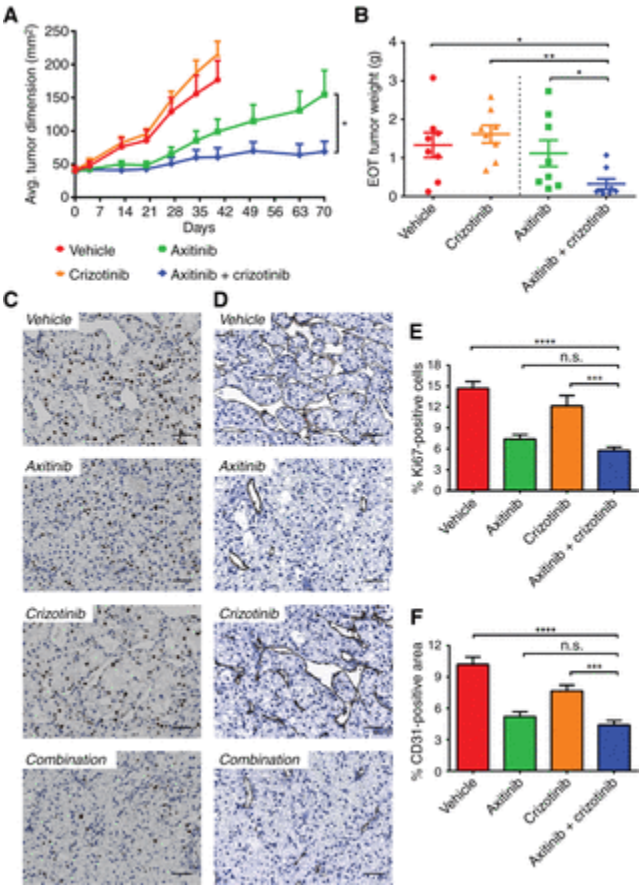

Figure 3.

Antitumor effect of axitinib and crizotinib in RP-R-01 ccRCC PDX (TKI-sensitive model). Subcutaneous RP-R-01–bearing mice (8 mice/group) were treated with vehicle, axitinib (36 mg/kg, 2×/day, 5×/week), crizotinib (25 mg/kg, 1×/day, 5×/week), or combination. A, tumor growth curve: each line represents the average tumor size (mm^2) of each treatment group ± SE. B, endpoint tumor weights (the vertical spotted line highlights the difference in time among groups). Tumors from treated mice were then harvested, processed, and tissue sections were stained for Ki67 (C) to evaluate proliferation and CD31 (D) for visualization of endothelial cells. E, blind quantitative analysis of Ki67, expressed as the mean percentage of positively stained nuclei ± SE and CD31 (F), expressed as the mean percentage of positively stained area ± SE; *, $P < 0.05$; **, $P < 0.01$; ***, $P < 0.001$; ****, $P < 0.0001$; n.s., not significant, as compared with the combination group, using two-tailed *t* test analysis.

Establishing a sunitinib-resistant RP-R-01 ccRCC PDX model

To mimic a TKIs resistant scenario, SCID mice were implanted with RP-R-01 tumor tissues. Sunitinib treatment (60 mg/kg, 1×/day, 5×/week, PO) started when tumors were detectable by caliper measurement (~25 mm^2) and continued until the average tumor dimension doubled (~50 mm^2), around day 112. At that time, we defined tumors as sunitinib resistant and mice were then randomly distributed into five experimental groups: either released from treatment ("vehicle"), maintained on sunitinib, switched to axitinib, to crizotinib or to axitinib plus crizotinib. Immunohistochemical comparison of sunitinib-sensitive and -resistant RP-R-01 tumors (harvested at day 112) indicated an increase in c-met expression (**Fig. 4A and B**) and a decrease in E-cadherin expression (**Fig. 4F and G**), suggesting a role of the HGF/c-met pathway in sunitinib-acquired resistance and a potential switch to a more mesenchymal phenotype. Increased c-met expression was paired with an increased activity of c-met RTK in the sunitinib-resistant tumors as suggested

by immunofluorescence detection of the phosphorylated $Tyr^{1230/1234/1235}$ in the c-met activation loop (P = 0.0453, **Fig. 4C and D**). Western blot analysis performed on three representative tumors per group confirmed the increase of c-met phosphorylation in the sunitinib-resistant experimental setting, and suggested not only an increase in the number of positive cells but also an overall increase of c-met activation (**Fig. 4E**).

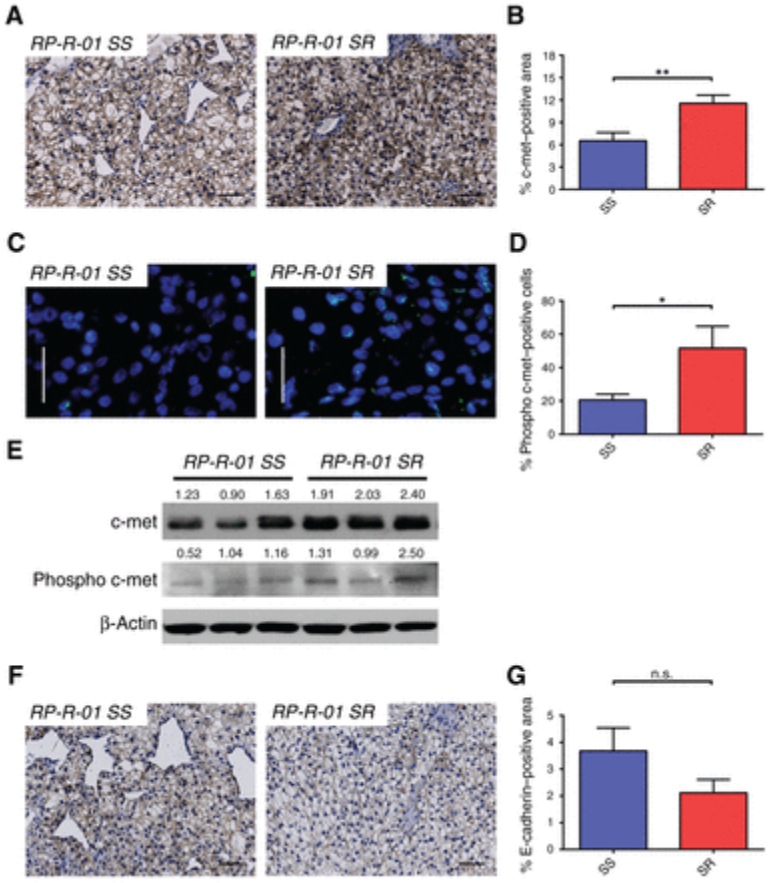

Figure 4.

RP-R-01 sunitinib-sensitive (SS) and -resistant (SR) histologic comparison. A, IHC staining of RP-R-01 sunitinib-sensitive and sunitinib-resistant (at day 112) tumor pieces with c-met; scale bar, 50 µm. B, blind quantitative analysis of c-met, expressed as the mean percentage of positively stained area ± SE. C, immunofluorescence staining of phosphorylated c-met (green), DAPI counterstain marks nuclei in blue; scale bar, 20 µm. D, blinded quantitative analysis of phosphorylated c-met, expressed as the mean percentage of positive cells ± SE. E, Western blot analysis of c-met expression and phosphorylation in lysates from three randomly selected RP-R-01 sunitinib-sensitive and -resistant tumor pieces. Numbers above bands, signal intensity normalized to respective loading control (β-actin). F, IHC staining of RP-R-01 sunitinib-sensitive and sunitinib-resistant tumor pieces with E-cadherin; scale bar, 50 µm. G, blinded quantitative analysis of E-cadherin, expressed as the mean percentage of positively stained area ± SE; *, P < 0.05; **, P < 0.01; n.s., not signficant, using two-tailed t test analysis.

Antitumor effect of axitinib and crizotinib in the sunitinib-resistant RP-R-01 PDX model

Despite an observed increase in c-met expression and phosphorylation, treatment with crizotinib did not result in tumor growth inhibition (**Fig. 5A**). On the other hand, mice either treated with axitinib or maintained on sunitinib showed significant inhibition of tumor growth as compared with mice taken off

treatment (tumor weight at day 151, end of treatment: $P = 0.0247$ vs. "vehicle" both axitinib or sunitinib, **Fig. 5B**). Once again, axitinib plus crizotinib combined treatment was more effective than continuous sunitinib treatment or switching to axitinib monotherapy (end of treatment tumor weight, $P = 0.0277$ vs. sunitinib and $P = 0.0133$ vs. axitinib). Ki67 immunostaining showed a strong increase of resistant tumor proliferation in mice taken off treatment as compared with tumors from mice maintained on sunitinib ($P = 0.0023$, **Fig. 6A and B**). Despite crizotinib treatment did not show any significant decrease in Ki67 staining, combination with axitinib decreased the percentage of proliferative nuclei to less than 5% ($P < 0.0001$). **Figure 6C** shows tumor blood vessel staining with CD31. Tumors released from sunitinib treatment were hypervascularized ($P = 0.0057$ "vehicle" vs. sunitinib) and this effect was reverted by both axitinib and crizotinib treatment ($P = 0.0035$ and $P = 0.0096$ vs. "vehicle," respectively). Combination treatment reduced tumor vascularization even more ($P = 0.0013$ vs. axitinib and $P = 0.0002$ vs. crizotinib, **Fig. 6D**). C-met expression by IHC did not show significant differences among experimental groups (data not shown). Though, the strong increase in c-met phosphorylation ($Tyr^{1230/1234/1235}$) in sunitinib- and axitinib-treated tumors was dramatically reduced by concomitant crizotinib treatment ($P = 0.0399$ vs. sunitinib and $P = 0.0149$ vs. axitinib single agent,**Fig. 6E and F**). Interestingly, single-agent crizotinib treatment was able to significantly reduce phosphorylated c-met expression, but this biologic effect was not associated with tumor growth inhibition. In accordance with the inhibition of the c-met pathway activity, crizotinib also induced a decrease in E-cadherin staining. However, this reduction was not associated with significant morphologic changes (Supplementary Fig. S4).

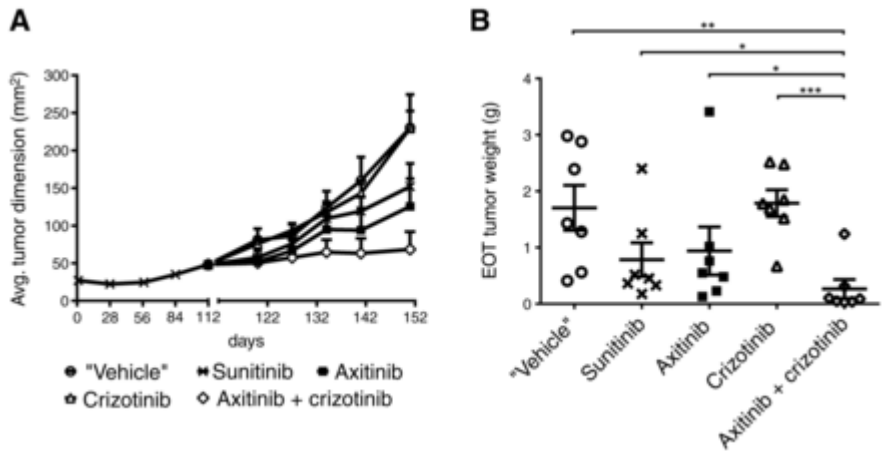

Figure 5.

Antitumor effect of axitinib and crizotinib in the sunitinib-resistant RP-R-01 ccRCC PDX. Subcutaneous RP-R-01–bearing mice (8 mice/group) were treated with sunitinib (60 mg/Kg, 1×/day, 5×/week) until tumor dimension doubled in size. Then, mice bearing tumors defined as sunitinib resistant were randomly distributed into five experimental groups: released from treatment ("vehicle"), maintained in sunitinib, axitinib (36 mg/kg, 2×/day, 5×/week), crizotinib (25 mg/kg, 1×/day, 5×/week), or axitinib plus crizotinib. A, tumor growth curve: each line represents the average tumor size (mm^2) of each treatment group ± SE. B, endpoint tumor weights; *, $P < 0.05$; **,$P < 0.01$; and ***, $P < 0.001$, as compared with the combination group, using two-tailed *t* test analysis.

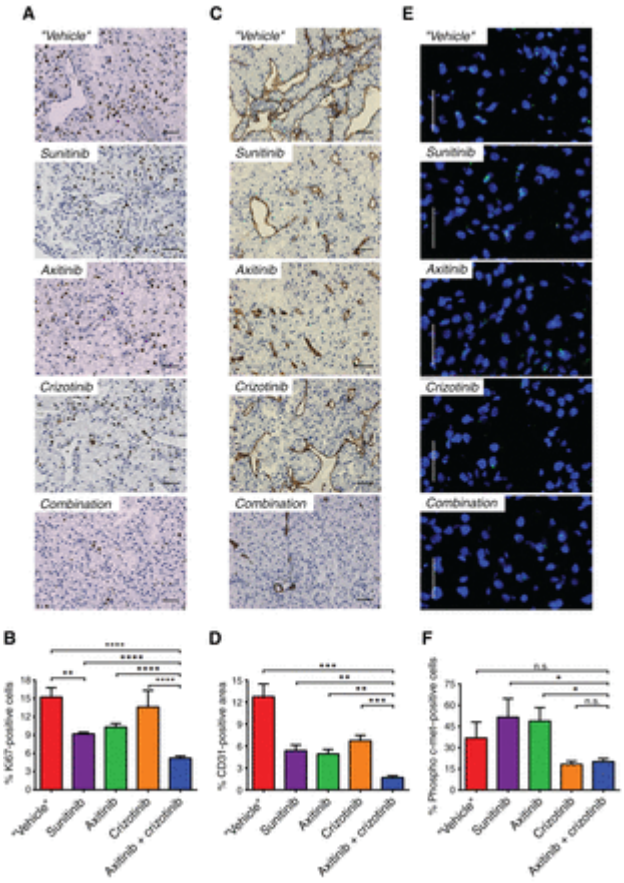

Figure 6.

Molecular effects of axitinib and crizotinib in the sunitinib-resistant RP-R-01 ccRCC PDX. Sunitinib-resistant RP-R-01–bearing mice treated as in **Fig. 4** were sacrificed after 5 months of treatment, tumors were harvested, processed, and tissue sections were stained for Ki67 (A) to evaluate proliferation, and CD31 (C) for visualization of endothelial cells. B, blinded quantitative analysis of Ki67, expressed as the mean percentage of positively stained nuclei ± SE, and CD31 (D), expressed as the mean percentage of positively stained area ± SE; scale bar, 50 µm. E, immunofluorescence staining of phosphorylated c-met (green), DAPI counterstain marks nuclei in blue; scale bar, 20 µm. F, blind quantitative analysis of phosphorylated c-met, expressed as mean the percentage of positive cells ± SE; *, $P < 0.05$; **, $P < 0.01$; ***, $P < 0.001$; ****, $P < 0.0001$; n.s., not significant, as compared with all other groups, using two-tailed *t* test analysis.

Discussion

Treatment of patients with ccRCC with TKIs, such as sunitinib, has been shown to induce significant clinical benefit and represents standard of care. However, inevitably tumor develops drug resistance and additional treatments are needed. Axitinib is a small molecule that inhibits VEGFRs activity with high specificity. In a phase III clinical trial, axitinib has been reported to significantly improve progression-free survival (PFS) compared with sorafenib and has been approved as second-line treatment in patients with advanced RCC (**9, 10**). In our RP-R-01 sunitinib-resistant model, the comparison between sunitinib and axitinib treatment did not show significant differences in terms of tumor growth and vascularization. This observation suggests that, at least in this model, inhibition of additional kinases (such as PDGFR and c-kit) may not provide advantage in tumor growth inhibition as compared with more selective VEGFR inhibition. On the other hand, we observed early onset of tumor resistance to anti–VEGF-targeted therapy in the 786-O model as previously reported (**24**). Interestingly, axitinib treatment in the 786-O orthotopic model

inhibited tumor vascularization but not tumor growth, and did not induce significant improvement in survival compared with vehicle. However, combination with crizotinib not only increased axitinib inhibition of tumor microvessel density, but also tumor growth and it improved survival. In this rapidly highly proliferative model, only when c-met inhibition and VEGFR blockade occurred concomitantly, the treatment led to tumor growth inhibition and improved survival.

The patient-derived xenograft developed in our laboratory, RP-R-01 (**21**) is a clinically relevant model of ccRCC because these tumors, by being passaged only *in vivo*, likely maintain the original heterogeneity that is often lost in tumor cell lines, and, more importantly, retain the clear cell morphology. In the short-term treatment experiment performed with this model, we noticed a significant reduction of blood vessels in axitinib-treated tumors in the absence of significant response in tumor growth. Blood vessels reduction in axitinib plus crizotinib group was even more significant, leading to a striking early induction of hypoxia following only 2 days of treatment. Moreover, a substantial increase in intratumor hypoxia in single-agent groups was detectable following 1-week treatment. HIF1α Western blot analysis also showed increased levels in the combination group following either short- or long-term treatment in the sunitinib-sensitive model, but significant decrease in the sunitinib-resistant tumors following long-term treatment (Supplementary Fig. S5A, S5B, and S5C). Interestingly, pimonidazole–CD31 dual staining pointed that treatment-induced hypoxia originates from the endothelial cells, suggesting a direct drug effect on the blood vessels. Furthermore, RP-R-01 tumors showed a strong response to VEGF-targeted therapies, and TKI resistance is a true acquired event that occurs after months of sunitinib treatment instead of the relatively short period displayed by tumor cell lines. To establish a TKI-resistant model, we treated RP-R-01–bearing mice with sunitinib (60 mg/kg, 1×/day, 5×/week) until, following a period of stabilization, the average tumor size doubled from baseline. In these sunitinib-resistant tumors, we observed an increase in c-met expression and activation as reported by other groups in glioblastoma, pancreatic neuroendocrine tumors, and other solid tumors (**16–18**, **23**). In contrast with the sunitinib-sensitive model, in the resistant RP-R-01 tumors we noticed a significant decrease in tumor vascularization in the combination group as compared with the axitinib-treated group, suggesting a role of c-met in blood vessels homeostasis. However, regardless of c-met expression and activity, crizotinib was not effective as single agent at the dose used, but it was able to significantly improve axitinib antitumor activity in both models. Furthermore, regardless of the inhibition of c-met phosphorylation following crizotinib treatment, tumor growth rate was similar to vehicle-treated tumors, suggesting a possible “rebound” effect when anti-VEGF therapy is halted (**25**), and the potential benefit of continuing VEGF blockade in patients despite radiologic signs of disease progression on initial TKIs. Overall, our data suggest that c-met inhibition is therapeutically effective in the setting of concomitant inhibition of VEGF in RCC models, without significant toxicity (Supplementary Fig. S6).

The molecular mechanisms responsible for c-met capability of compensating VEGF inhibition in RCC remain to be elucidated. One possibility is that the c-met/HGF pathway has a stronger role in tumor endothelial and stromal cells, in which it acts as a potent proangiogenic trigger, supporting tumor growth. In fact, HGF is a well-known inducer of endothelial cell proliferation, survival and migration, and a chemoattractant for proangiogenic bone marrow–derived progenitor cells (**26**). These changes in the tumor microenvironment may foster angiogenesis, leading to tumor growth regardless of the status of c-met expression in the tumor. It has been shown that treatment with a decoy c-met not only delays the growth of c-met–positive xenografts, but also the growth of c-met–negative tumors (**27**). This observation could explain our findings showing the lack of association between the effect of crizotinib and c-met expression in cancer cells. A second hypothesis is that anti-VEGF therapies eliminate basal c-met inhibition as demonstrated by Lu and colleagues (**16**). A model of glioblastoma multiforme showed a direct VEGFR2 physical association with c-met that led to its posttranslational inactivation. In this context, VEGF blockade abrogated the suppression

of c-met phosphorylation, activating the c-met/HGF pathway directly in cancer cells. Finally, c-met transcriptional activation could directly lead to survival benefit and prevent from apoptosis in a VEGF inhibition context, as demonstrated following EGFR inhibition by gefitinib (**28**).

There are emerging clinical data, suggesting that c-met represents a potential target for therapeutic intervention. In a recent phase I clinical trial treatment with cabozantinib, a dual c-met and VEGFR inhibitor, has been shown to induce a 30% objective response rate and a PFS of 14.7 months in patients with prior VEGF or mTOR inhibitors (**29**). These promising results have led to the further clinical development of cabozantinib in patients with recurrent RCC both in first-line setting and following TKIs. Our preclinical data did not identify an optimal setting (TKI-sensitive vs. TKI-resistant disease) for the introduction of c-met inhibition. The challenge is represented by the fact that, at least under our experimental conditions, tumor c-met expression does not seem to be predictive of response to a selective inhibitor. Future preclinical and clinical testing of c-met inhibitors will define the role of these agents in the armamentarium available to effectively treat recurrent RCC.

In conclusion, to our knowledge, this study is the first preclinical evidence of the key role of c-met in response to anti-VEGF therapy in ccRCC by using different models. Overall, our results highlight the potential therapeutic combination of VEGF and HGF/c-met pathway inhibition in the treatment of ccRCC, both in the first- and second-line setting and independently from constitutively overexpressed c-met in tumor cells.

Disclosure of Potential Conflicts of Interest

R. Pili reports receiving a commercial research grant and is a consultant/advisory board member for Pfizer. No potential conflicts of interest were disclosed by the other authors.

Authors' Contributions

Conception and design: E. Ciamporcero, K.M. Miles, L. Shen, S. Pizzimenti, R. Pili

Development of methodology: E. Ciamporcero, K.M. Miles, S.Y. Ku, R. Pili

Acquisition of data (provided animals, acquired and managed patients, provided facilities, etc.): E. Ciamporcero, K.M. Miles, R. Adelaiye, R. Pili

Analysis and interpretation of data (e.g., statistical analysis, biostatistics, computational analysis): E. Ciamporcero, R. Adelaiye, R. Pili

Writing, review, and/or revision of the manuscript: E. Ciamporcero, L. Shen, S. Pizzimenti, B. Sennino, R. Pili

Administrative, technical, or material support (i.e., reporting or organizing data, constructing databases): S. Ramakrishnan, L. Shen, B. Sennino, R. Pili

Study supervision: G. Barrera, R. Pili

Grant Support

This research was supported in part by the National Cancer Institute, NIH (P30CA016056; to R. Pili), and by a research grant from Pfizer (to R. Pili).

The costs of publication of this article were defrayed in part by the payment of page charges. This article must therefore be hereby marked *advertisement* in accordance with 18 U.S.C. Section 1734 solely to indicate this fact.

Acknowledgments

The authors thank the MTMR and Pathology Core Facilities at RPCI for animal handling and processing the tissue samples.

References

1.

1. Siegel R,
2. Naishadham D,
3. Jemal A

. Cancer statistics, 2013. CA Cancer J Clin 2013;**63**:11–30.

2.

1. Rini BI,
2. Campbell SC,
3. Escudier B

. Renal cell carcinoma. Lancet 2009;**373**:1119–32.

3.

1. Baldewijns MM,
2. van Vlodrop IJH,
3. Vermeulen PB,
4. Soetekouw PMMB,
5. van Engeland M,
6. de Bruïne AP

. VHL and HIF signalling in renal cell carcinogenesis. J Path 2010;**221**:125–38.

4.

1. Oh RR,
2. Park JY,
3. Lee JH,

4. Shin MS,
5. Kim HS,
6. Lee SK,
7. et al.

Expression of HGF/SF and Met protein is associated with genetic alterations of VHL gene in primary renal cell carcinomas. Acta Pathol Microbiol Immunol Scand 2002;**110**:229–38.

5.

1. Pennacchietti S,
2. Michieli P,
3. Galluzzo M,
4. Mazzone M,
5. Giordano S,
6. Comoglio PM

. Hypoxia promotes invasive growth by transcriptional activation of the met protooncogene. Cancer Cell 2003;**3**:347–61.

6.

1. Hicklin DJ,
2. Ellis LM

. Role of the vascular endothelial growth factor pathway in tumor growth and angiogenesis. J Clin Oncol 2005;**23**:1011–27.

7.

1. Ellis LM,
2. Hicklin DJ

. VEGF-targeted therapy: mechanisms of anti-tumour activity. Nature Rev Cancer2008;**8**:579–91.

8.

1. Faivre S,
2. Demetri G,
3. Sargent W,
4. Raymond E

. Molecular basis for sunitinib efficacy and future clinical development. Nature Rev Drug Discov 2007;**6**:734–45.

9.

1. Rini BI,
2. Escudier B,
3. Tomczak P,
4. Kaprin A,
5. Szczylik C,
6. Hutson TE,
7. et al.

Comparative effectiveness of axitinib versus sorafenib in advanced renal cell carcinoma (AXIS): a randomised phase 3 trial. Lancet2011;**378**:1931–9.

10.

1. Motzer RJ,
2. Escudier B,
3. Tomczak P,
4. Hutson TE,
5. Michaelson MD,
6. Negrier S,
7. et al.

Axitinib versus sorafenib as second-line treatment for advanced renal cell carcinoma: overall survival analysis and updated results from a randomised phase 3 trial. Lancet Oncol 2013;**14**:552–62.

11.

1. Hu-Lowe DD,
2. Zou HY,
3. Grazzini ML,
4. Hallin ME,
5. Wickman GR,
6. Amundson K,

7. et al.

Nonclinical antiangiogenesis and antitumor activities of axitinib (AG-013736), an oral, potent, and selective inhibitor of vascular endothelial growth factor receptor tyrosine kinases 1, 2, 3. Clin Cancer Res 2008;**14**:7272–83.

12.

1. Bergers G,
2. Hanahan D

. Modes of resistance to anti-angiogenic therapy. Nature Rev Cancer2008;**8**:592–603.

13.

1. Sennino B,
2. McDonald DM

. Controlling escape from angiogenesis inhibitors. Nat Rev Cancer2012;**12**:699–709.

14.

1. Trusolino L,
2. Bertotti A,
3. Comoglio PM

. MET signalling: principles and functions in development, organ regeneration and cancer. Nat Rev Mol Cell Biol 2010;**11**:834–48.

15.

1. Danilkovitch-miagkova A,
2. Zbar B

. Dysregulation of Met receptor tyrosine kinase activity in invasive tumors. J Clin Invest 2002;**109**:863–7.

16.

1. Lu K V,
2. Chang JP,
3. Parachoniak CA,
4. Pandika MM,
5. Aghi MK,
6. Meyronet D,

7. et al.

VEGF inhibits tumor cell invasion and mesenchymal transition through a MET/VEGFR2 complex. Cancer Cell 2012;**22**:21–35.

17.

1. Jahangiri A,
2. De Lay M,
3. Miller LM,
4. Carbonell WS,
5. Hu Y-L,
6. Lu K,
7. et al.

Gene expression profile identifies tyrosine kinase c-Met as a targetable mediator of antiangiogenic therapy resistance. Clin Cancer Res2013;**19**:1773–83.

18.

1. Shojaei F,
2. Lee JH,
3. Simmons BH,
4. Wong A,
5. Esparza CO,
6. Plumlee Pa,
7. et al.

HGF/c-Met acts as an alternative angiogenic pathway in sunitinib-resistant tumors. Cancer Res 2010;**70**:10090–100.

19.

1. Zou HY,
2. Li Q,
3. Lee JH,
4. Arango ME,
5. McDonnell SR,

6. Yamazaki S,
7. et al.

An orally available small-molecule inhibitor of c-Met, PF-2341066, exhibits cytoreductive antitumor efficacy through antiproliferative and antiangiogenic mechanisms. Cancer Res 2007;**67**:4408–17.

20.

1. Shaw AT,
2. Kim D-W,
3. Nakagawa K,
4. Seto T,
5. Crinó L,
6. Ahn M-J,
7. et al.

Crizotinib versus chemotherapy in advanced ALK-positive lung cancer. NEJM 2013;**368**:2385–94.

21.

1. Hammers HJ,
2. Verheul HM,
3. Salumbides B,
4. Sharma R,
5. Rudek M,
6. Jaspers J,
7. et al.

Reversible epithelial to mesenchymal transition and acquired resistance to sunitinib in patients with renal cell carcinoma: evidence from a xenograft study. Mol Cancer Ther 2010;**9**:1525–35.

22.

1. Tuominen VJ,
2. Ruotoistenmäki S,
3. Viitanen A,
4. Jumppanen M,
5. Isola J

. ImmunoRatio: a publicly available web application for quantitative image analysis of estrogen receptor (ER), progesterone receptor (PR), and Ki-67. Breast Cancer Res 2010;**12**:R56.

23.

1. Sennino B,
2. Ishiguro-Oonuma T,
3. Wei Y,
4. Naylor RM,
5. Williamson CW,
6. Bhagwandin V,
7. et al.

Suppression of tumor invasion and metastasis by concurrent inhibition of c-Met and VEGF signaling in pancreatic neuroendocrine tumors. Cancer Discov 2012;**2**:270–87.

24.

1. Bhatt RS,
2. Wang X,
3. Zhang L,
4. Collins MP,
5. Signoretti S,
6. Alsop DC,
7. et al.

Renal cancer resistance to antiangiogenic therapy is delayed by restoration of angiostatic signaling. Mol Cancer Ther 2010;**9**:2793–802.

25.

1. Mancuso MR,
2. Davis R,
3. Norberg SM,
4. O'Brien S,
5. Sennino B,
6. Nakahara T,

7. et al.

Rapid vascular regrowth in tumors after reversal of VEGF inhibition. J Clin Invest 2006;**116**:2610–21.

26.

1. Bussolino F,
2. Di Renzo MF,
3. Ziche M,
4. Bocchietto E,
5. Olivero M,
6. Naldini L,
7. et al.

Hepatocyte growth factor is a potent angiogenic factor which stimulates endothelial cell motility and growth. J Cell Biol1992;**119**:629–41.

27.

1. Michieli P,
2. Mazzone M,
3. Basilico C,
4. Cavassa S,
5. Sottile A,
6. Naldini L,
7. et al.

Targeting the tumor and its microenvironment by a dual-function decoy Met receptor. Cancer Cell 2004;**6**:61–73.

28.

1. Jun HJ,
2. Acquaviva J,
3. Chi D,
4. Lessard J,
5. Zhu H,
6. Woolfenden S,

7. et al.

Acquired MET expression confers resistance to EGFR inhibition in a mouse model of glioblastoma multiforme. Oncogene 2012;**31**:3039–50.

29.

1. Choueiri T,
2. Pal SK,
3. McDermott DF,
4. Morrissey S,
5. Ferguson KC,
6. Holland J,
7. et al.

A phase I study of cabozantinib (XL184) in patients with renal cell cancer. Ann Oncol 2014;**8**:1603–8.